Electrochimica Acta 453 (2023) 142349

Contents lists available at ScienceDirect

Electrochimica Acta

journal homepage: www.journals.elsevier.com/electrochimica-acta

# Highly conductive polyacrylonitrile-based hybrid aqueous/ionic liquid solid polymer electrolytes with tunable passivation for Li-ion batteries

Kyle B. Ludwig [a], Riordan Correll-Brown [a], Max Freidlin [a], Mounesha N. Garaga [b], Sahana Bhattacharyya [a], Patricia M. Gonzales [a], Arthur V. Cresce [c], Steve Greenbaum [b], Chunsheng Wang [a], Peter Kofinas [a,*]

[a] Department of Chemical & Biomolecular Engineering, University of Maryland, 4418 Stadium Dr., College Park, MD 20740, USA
[b] Department of Physics & Astronomy, Hunter College of the City University of New York, 695 Park Ave., New York, NY 10065, USA
[c] Combat Capabilities Development Command US Army Research Laboratory, 2800 Powder Mill Rd., Adelphi, MD 20783, USA

ARTICLE INFO

*Keywords:*
Polymer electrolytes
Aqueous electrolytes
Ionic liquids
Ionic conductivity
Passivation

ABSTRACT

The rapid growth in demand for lithium-ion batteries that can deliver more energy and power has generated concerns over safety. Aqueous electrolytes are a strong candidate to alleviate this apprehension, however their ability to overcome the "cathodic challenge" is limited due to anion-dominated passivation at the anode. In this work, the recently developed "hybrid aqueous/nonaqueous" electrolyte (HANE) strategy was employed to tune the degree of passivation at the anode in solid polymer electrolytes (SPEs) by using various ionic liquids as the nonaqueous component. Whereas common HANE systems sacrifice ionic conductivity to create a more robust passivation layer at the cathodic limit, the "hybrid aqueous/ionic liquid" SPEs (HAILSPEs) investigated in this work do not. Two HAILSPE systems (H1, H2.5) were fabricated from a blend of polyacrylonitrile (PAN), water, lithium bis(trifluoromethylsulfonyl)imide (LiTFSI), and either triethylsulfonium-TFSI ($S_{2,2,2}$) or *N*-methyl-*N*-propylpyrrolidinium-TFSI ($Pyr_{1,3}$). These HAILSPE systems demonstrated a remarkable improvement in transport properties compared to their predecessors, achieving room temperature ionic conductivities of up to 5.39 mS/cm. A reduction in apparent activation energy and nearly complete decoupling of ionic transport from polymer chain mobility were found to contribute to this increase. Stable and complete growth of a passivating layer at 2 V vs. $Li/Li^+$ was also observed, which was tuned by changing the ionic liquid. The work presented here provides a potential route for overcoming the "cathodic challenge" in aqueous SPEs.

## 1. Introduction

More than 30 years after the production of the first commercial lithium-ion battery (LIB), they have become a ubiquitous part of everyday life; from portable electronics and electric vehicles to aerospace and largescale grid storage applications [1–4]. Despite decades of research and progress, the demand for systems with higher energy densities, higher voltage outputs, greater rate capabilities, and lower cost is outpacing the discovery of new battery chemistries [5–9]. As a result, concerns for safety have become widespread following high-profile failures [10]. In response, a growing field of research investigating safer alternatives to replace the flammable and often electrochemically unstable organic liquid electrolytes used in commercial LIBs has bloomed [11–13]. To this end, solid polymer electrolytes (SPEs) have garnered attraction because they are generally nonflammable and address several battery failure modes, including leaking, overcharging, and elevated temperatures [14]. However, the ionic conductivity and cation transport number of SPEs are generally limited ($10^{-4}$—$10^{-6}$ S/cm, <0.4) due to polymer crystallinity in traditional poly (ethylene oxide) (PEO) based systems [15–17].

Efforts to compensate for the poor performance of SPEs have focused on introducing plasticizers such as ceramic particles, ionic liquids, and water into electrolyte systems [18–21]. Plasticizers allow for less restricted diffusion of lithium ions ($Li^+$) by suppressing crystallinity through disruption of inter- and intra-molecular forces and expansion of the free-volume between polymer chains. In aqueous SPE (ASPE) systems, it has been shown that even a small amount of water acts as a strong plasticizer and unlocks an alternative pathway for ionic

* Corresponding author.
*E-mail address:* kofinas@umd.edu (P. Kofinas).

https://doi.org/10.1016/j.electacta.2023.142349
Received 3 March 2023; Received in revised form 28 March 2023; Accepted 31 March 2023
Available online 1 April 2023

conduction that significantly improves the transport of $Li^+$ [20]. Based on the "water-in-salt" electrolyte (WiSE) developed by Suo and co-authors in 2015, these ASPEs demonstrated a large degree of decoupling between ionic transport and polymer chain mobility, evident from high room temperature ionic conductivities up to 1.75 mS/cm and lithium-ion dominated transport ($D_{Li^+} > D_{TFSI^-}$) with lithium-ion transport numbers ($t_{Li^+}$) of ~ 0.65. Despite the favorable transport properties observed in the ASPE systems, the benefit of anion-derived passivation and solid electrolyte interphase (SEI) formation in superconcentrated systems was not fully realized. As observed in the WiSE, expansion of the ASPE cathodic limit was minimal due to the repulsion of bis(trifluoromethylsulfonyl)imide anions ($TFSI^-$) by negatively polarized anode surfaces. This "cathodic challenge" makes it difficult for $TFSI^-$ to reduce and contribute to SEI formation [22]. For this reason, increasing the lithium salt concentration also proves to be ineffective at expanding the cathodic limit [23].

Recently, a new class of "hybrid aqueous/nonaqueous" electrolyte (HANE) has been reported by several groups [24–26]. HANEs utilize an additional nonaqueous – often organic – component to assist in interphase formation and extend stability. This results in a system that combines the nonflammability, non-toxicity, and relatively fast transport properties of aqueous electrolytes with robust SEI formation at the anode due to both $TFSI^-$ and nonaqueous solvent reduction. For Wang and coauthors, this strategy resulted in further reduction of the cathodic limit from 1.9 V vs. $Li/Li^+$ in their previous WiSE system to 1.0 V vs. $Li/Li^+$ in their HANE system [24,27]. Although the HANE displayed improved stability through the inclusion of dimethyl carbonate, the ionic conductivity was reduced by nearly half. To this end, we report here a new class of SPE system inspired by the HANE strategy that demonstrates tunable stability without sacrificing transport properties. In lieu of organic solvents, ionic liquids were used to create "hybrid aqueous/ionic liquid" SPEs (HAILSPEs). The inclusion of ionic liquids aided in the nearly complete decoupling of ionic transport and polymer chain mobility, with electrolytes exhibiting room temperature ionic conductivity values >2.31 mS/cm. This improvement from the prior ASPE systems was found to be due to a reduction in the apparent activation energy of the systems to <0.30 eV. This has significant implications, as even a modest 10% decrease in activation energy can drastically increase ionic conductivity by more than 300% at a given temperature. The HAILSPEs were found to have activation energies comparable to those of liquid electrolytes such as the WiSE (0.286 eV) or the HANE (0.228 eV) and demonstrated improved transport of $Li^+$ in some compositions which increased $t_{Li^+}$ to 0.75. These improvements in transport properties were found to be primarily caused by minor changes in electrolyte composition rather than the choice between triethylsulfonium-TFSI ($S_{2,2,2}$) or *N*-methyl-*N*-propylpyrrolidinium-TFSI ($Pyr_{1,3}$) as the ionic liquid. However, the propensity to form a protective interphase at the anode was found to be highly dependent on choice of ionic liquid chemistry, with $S_{2,2,2}$ electrolytes offering better protection against $H_2O$ reduction than their $Pyr_{1,3}$ analogs. Nevertheless, the HAILSPE systems investigated here all showed SEI growth that culminated in complete surface coverage within the first 5 cycles. This approach provides inspiration to develop strategies for tuning passivation without sacrificing transport properties by modifying the chemistry of the ionic liquid cation.

## 2. Experimental

### 2.1. Materials

Polyacrylonitrile powder (PAN, $\overline{M}_w$ = 230,000 Da) was purchased from Goodfellow Corporation. $S_{2,2,2}$ and lithium-TFSI (LiTFSI) were purchased from Sigma Aldrich. $Pyr_{1,3}$ was purchased from Solvionic. These materials were stored inside a desiccator in a dry environment under vacuum when not in use. 304 stainless steel CR2032 coin cell parts (cases, spacers, wave springs), heat-sealable laminated aluminum pouch film, and 201 nickel ribbon were purchased from MTI Corporation. Polytetrafluoroethylene (PTFE) film (t = 0.25 mm) was purchased from McMaster-Carr. Titanium foil (t = 0.025 mm) was purchased from Goodfellow Corporation. Lithium iron phosphate (LFP) electrode sheets (32.5 × 92.5 mm) on aluminum were obtained from Electrodes and More. Graphite electrode sheets on copper were obtained from Argonne National Laboratory. Separator material was obtained from Asahi Kasei. LP57 electrolyte (1 M $LiPF_6$ in 3:7 v/v EC:EMC) was obtained from Gotion. These materials were stored and handled in a humidity-controlled dry room (relative humidity <1%) or glovebox (MBRAUN) with an argon atmosphere.

### 2.2. HAILSPE preparation

HAILSPEs were prepared via a solvent-free hot-pressing process. First, PAN, deionized $H_2O$, ionic liquid ($S_{2,2,2}/Pyr_{1,3}$), and LiTFSI were mixed in the appropriate amounts using a mortar and pestle. The resulting solid mixture was heat-sealed between two sheets of PTFE inside a laminated aluminum pouch to prevent changes in the water content of the electrolyte. The pouch was then pressed at ~130 °C, above the glass transition temperature ($T_g$) of PAN, for 1 min with a force of 1 metric ton using a Carver press, resulting in a homogeneous film with thickness of 100—200 μm, depending on the composition. These films were further processed for specific experiments, outlined below.

### 2.3. Electrochemical characterization

#### 2.3.1. Electrochemical impedance spectroscopy

Impedance measurements were performed on a Solartron 1287A/1255B platform. HAILSPEs were placed in a symmetrical coin cell using 304 stainless steel blocking electrodes then annealed at 60 °C for 24 h. A 0.25 mm thick PTFE spacer with a 4 mm inner diameter was used to create a clean, well-defined area of contact between the two blocking electrodes. Electrochemical impedance spectroscopy (EIS) was measured from 1 MHz to 1 Hz with a 10 mV amplitude over a range of temperatures from 0 °C to 80 °C in increments of 5 °C, including a one-hour dwell time between each temperature to allow the electrolyte to equilibrate. The samples were made using an empirically determined amount of electrolyte that best fills the volume defined by the PTFE spacer, outlined in a previous work [19]. Following measurement, all data were analyzed using a specific error model and linear regression outlined in the Supplemental Information.

#### 2.3.2. $L_{0.5}FP$ reference/counter electrode preparation

Due to the constraints of SPEs that limit compatibility with standard reference electrodes in three-electrode configurations, a suitable reference/counter electrode material for two-electrode voltammetry experiments was developed. A porous LFP was chosen because of its wide voltage stability and high surface area that make it both a good reference and counter electrode material. To ensure the stability of the reference electrode's voltage during voltammetry, where it will experience changing degrees of lithiation, the LFP was charged to precisely one-half of its discharge capacity. At this point, which lies directly in the middle of the voltage plateau, a perturbation in the state of charge – in either direction – will have a minimized effect on the voltage.

To prepare half-charged LFP ($L_{0.5}FP$), pouch cells were constructed with LFP/separator/graphite and filled with enough LP57 electrolyte to fully wet the separator. Prior to assembly, the LFP and graphite electrodes were tabbed with nickel ribbon using a Sonobond ultrasonic metal spot welder, then allowed to dry in a vacuum oven at 100 °C for 24 h. The pouch cells were vacuum sealed (30 s, -30 psig) after filling. A Maccor 4000-series was used to complete a two-step process: the pouch cell was first cycled at 1C from 2.7 to 3.8 V for two cycles to find the discharge capacity ($DC_2$), and then fully charged and discharged at C/5

from 2.7 to 3.8 V before finally charging again at C/5 to $DC_2/2$ (Fig. S2). Following the half-charging procedure, the $L_{0.5}FP$ was extracted, washed thoroughly with dry dimethyl carbonate to remove any remaining electrolyte, and then allowed to dry in a vacuum oven at 100 °C for 24 h.

#### 2.3.3. Linear sweep voltammetry and cyclic voltammetry

Linear sweep voltammetry (LSV) and cyclic voltammetry (CV) were performed on a Solartron 1287A/1255B platform. $L_{0.5}FP$/HAILSPE/Ti coin cells were constructed and then annealed at 60 °C for 24 h. A 0.25 mm thick PTFE spacer with a 6.35 mm inner diameter was used to create a clean, well-defined area of contact between the $L_{0.5}FP$ and Ti working electrode. The coin cells were equilibrated at 25 °C for one hour prior to measurement and then swept at a scan rate of 0.5 mV/s. For LSV, the cell was swept from the open circuit voltage (OCV) to arbitrarily high and low potentials; either 6.425 V vs. $Li/Li^+$ (3 V vs. reference, oxidative) or -0.575 V vs. $Li/Li^+$ (-4 V vs. reference, reductive). In the analogous oxidative CV measurement, the cell was swept from the OCV to 5 V vs. $Li/Li^+$ (1.575 V vs. reference) and then back to 3.425 V vs. $Li/Li^+$ (0 V vs. reference) for one cycle, for at least five total cycles. In the analogous reductive CV measurement, the cell was swept from the OCV to 1.925 V vs. $Li/Li^+$ (-1.50 V vs. reference) and then back to 3.425 V vs. $Li/Li^+$ (0 V vs. reference) for one cycle, for at least five total cycles. The measured current response was converted to a current density by dividing by the area of the PTFE spacer (31.67 $mm^2$).

### 2.4. Material characterization

#### 2.4.1. Thermogravimetric analysis

The water content of all electrolytes was determined via thermogravimetric analysis (TGA) using a Shimadzu TGA-50 with a TA-60WS interface and FC-60A flow controller. Samples were prepared by loading 15—25 mg of electrolyte in an alumina crucible. Samples were heated at a rate of 10 °C/min from room temperature to 150 °C, then held isothermally for 45 min. A flowrate of 50 mL/min of high purity nitrogen gas (Airgas, Inc.) was used. The instrument's accompanying software was used to calculate the percent mass lost by taking the difference between the initial ($t = 0$ min) and equilibrated ($t > 55$ min) sample mass. The mass loss was attributed entirely to water in the system since LiTFSI, $S_{2,2,2}$, and $Pyr_{1,3}$ have no vapor pressure and the degradation temperature of PAN is >150 °C. The relative amount of water absorbed during electrolyte processing and handling was calculated by

$$M_{H_2O,absorbed} = \frac{x}{100}(53.06N_{PAN} + 18.02N_{H_2O} + MW_{IL}N_{IL} + 287.10N_{LiTFSI}) - \frac{18.02N_{H_2O}}{1-(x/100)} \quad (1)$$

where $x$ is the percent mass loss measured from TGA, $MW_{IL}$ is the molar mass of the respective ionic liquid ($S_{2,2,2}$TFSI/$Pyr_{1,3}$TFSI), and $N_{PAN}$, $N_{H_2O}$, $N_{IL}$, and $N_{LiTFSI}$ are the designated molar amounts of PAN, $H_2O$, ionic liquid, and LiTFSI for the composition. The final relative amount of water in the electrolyte was calculated by

$$N_{H_2O,total} = N_{H_2O} + \frac{M_{H_2O,absorbed}}{18.02}. \quad (2)$$

This final water content accurately describes all the electrolytes, including those measured with EIS, DSC, LSV, and CV since all samples and cells were constructed at the same time and contain the same amount of water after absorption.

#### 2.4.2. Differential scanning calorimetry

Modulated differential scanning calorimetry (mDSC) was performed on a TA Instruments Q2500 differential scanning calorimeter. Samples were prepared by hermetically sealing 10—15 mg of electrolyte in an aluminum pan. Samples were cooled from room temperature to -70 °C, allowed to equilibrate, then heated to 110 °C at a rate of 3 °C/min with a ±1 °C/min modulation. A flowrate of 50 mL/min of high purity nitrogen gas (Airgas, Inc.) was used. The reversible heat flow data and any calculated transitions were exported from the accompanying TRIOS software.

#### 2.4.3. Pulsed-field gradient nuclear magnetic resonance (pfg-NMR)

All electrolytes were opened and packed into NMR tubes (5 × 180 mm), following the procedure outlined in Fig. S3, on the same day within a limited amount of time to ensure exposure to a constant ambient atmosphere. The NMR tubes were subsequently sealed to preserve the atmosphere in which they were prepared, preventing any flux of water into or out of the tube. The diffusion coefficients for $TFSI^-$ ($^{19}F$) and $Li^+$ ($^7Li$) were measured on a 300 MHz Varian-S Direct Drive Wide Bore Nuclear Magnetic Resonance (NMR) spectrometer operating at a magnetic field of 7 T ($^{19}F$ and $^7Li$ Larmor frequencies of 284.4 and 117 MHz, respectively) equipped with a Doty Scientific Z-spec pulsed-field gradient probe (DS-1034). The diffusion coefficients for $H_2O$ and $IL^+$ ($^1H$) were also measured on a 300 MHz NMR spectrometer ($^1H$ Larmor frequency of 300 MHz) for the two "H2.5" electrolytes. The diffusion coefficients for $H_2O$ and $IL^+$ ($^1H$) in the two "H1" electrolytes were measured on a 400 MHz Bruker NMR spectrometer operating at 9.39 T ($^1H$ Larmor frequency of 401 MHz). The signal was accumulated over 16 transients with an optimized recycling delay of 2—3.5 s in the Varian spectrometer and 2—3 s in the Bruker spectrometer. The diffusion coefficients were measured at room temperature (25 °C) by using a spinecho pulse sequence. The gradient strength, $G$, was varied in the range of 3—841 G/cm (Varian) and 0.5—50 G/cm (Bruker) for 16 increments. The diffusion time, Δ, and the diffusion pulse length, $\delta$, were set to 10—100 ms and 2—3 ms, respectively, for the Varian spectrometer, and 600—900 ms and 8—12 ms, respectively, for the Bruker spectrometer. From each experiment, the integrated signal strength, $S$, as a function of the applied gradient was obtained, and the diffusion coefficients, $D$, were calculated by using least-squares monoexponential ($^{19}F$, $^7Li$) or biexponential ($^1H$) fitting of the Stejskal-Tanner equation, given by

$$S = S_0 exp^{-D(G\delta\gamma)^2\left(\Delta - \left(\frac{\delta}{3}\right)\right)} \quad (3)$$

where $S_0$ is the signal strength without a diffusion gradient pair and $\gamma$ is the nuclear gyromagnetic ratio of the corresponding nucleus (Fig. S4) [20,28].

## 3. Results and discussion

In this study, four HAILSPE systems were fabricated and characterized: two different compositions HAILSPE-1 and HAILSPE-2.5 (H1 and H2.5), each with two different ionic liquids $S_{2,2,2}$ and $Pyr_{1,3}$. H1 and H2.5 differ only by the amount of ionic liquid; H1 contains 1 part ionic liquid whereas H2.5 contains 2.5 parts ionic liquid, when compared to the other components. The electrolytes follow the nomenclature of first identifying the ionic liquid used and then identifying the composition that describes the molar ratio of each component (e.g., "$S_{2,2,2}$ H1"). Fig. S1 gives the molecular structure, atomic mass, and van der Waals volume for the TFSI anion and each of the ionic liquid cations used in the HAILSPE systems, as well as several optical images of the electrolytes. The relative final compositions of the electrolytes are given in Tables 1 and 2 for different experimental measurements as molar ratios of each of the components; 6.14 parts PAN, 14.96—29.34 parts $H_2O$, 1 or 2.5 parts ionic liquid, and 6.93 parts LiTFSI. The relative molar ratio of PAN is of the repeat unit which allows the analyses presented to be independent of polymer molecular weight, offering better insight into the effect of water and ionic liquid on electrolyte properties.

PAN was selected because its strong oxidative stability circumvents

**Table 1**
Summary of the properties determined from EIS and Arrhenius regression for the four HAILSPE systems investigated. The compositions of the electrolyte are provided and represent molar ratios.

| | PAN | $H_2O$ | IL | LiTFSI | $\sigma_{25^\circ C}$ mS cm$^{-1}$ | ln*A* | $E_a$ kJ mol$^{-1}$ | $E_a$ eV | $R^2$ |
|---|---|---|---|---|---|---|---|---|---|
| **$S_{2,2,2}$ H1** | 6.14 | 14.96 | 1 | 6.93 | 2.31 | 5.79 | 29.60 | 0.307 | 0.9889 |
| **$Pyr_{1,3}$ H1** | 6.14 | 24.44 | 1 | 6.93 | 4.55 | 6.30 | 29.12 | 0.302 | 0.9939 |
| **$S_{2,2,2}$ H2.5** | 6.14 | 29.09 | 2.5 | 6.93 | 5.01 | 4.11 | 23.45 | 0.243 | 0.9926 |
| **$Pyr_{1,3}$ H2.5** | 6.14 | 29.34 | 2.5 | 6.93 | 5.39 | 6.14 | 28.20 | 0.292 | 0.9938 |

the thermodynamic instability at 4 V vs. $Li/Li^+$ commonly seen in PEO-based SPEs, which is due to the oxidation of the electron-rich ether oxygens [13,29]. Furthermore, nitrile-functional polymers like PAN are excellent Lewis bases that can coordinate to and solvate $Li^+$ and PAN-based SPEs have shown enhanced anodic limits ~ 5.5 V vs $Li/Li^+$ [30–32]. The molecular weight of PAN ($\overline{M}_w$ = 230,000 Da) was chosen to be as high as commercially available to ensure solid-like properties in the HAILSPE compositions that can contain varying degrees of water and ionic liquid. $TFSI^-$ was chosen as the anion for both the lithium salt and ionic liquids for its chemical and thermal stability, ease of dissociation, and ability to contribute to LiF formation in the SEI [27,33–35]. $S^+_{2,2,2}$ was chosen as a cation of interest based on our previous work on a nonaqueous ionic liquid SPE (ILSPE), which showed that inclusion of $S_{2,2,2}$ and LiTFSI in a PEO matrix established the propensity to improve ionic conductivity by plasticizing the polymer network to reduce crystallinity [19]. CV, lithium metal stripping and plating, and galvanostatic cycling measurements also indicated strong passivating behavior and interfacial stability at low voltages. $Pyr^+_{1,3}$ was chosen as an additional cation of interest because it has been extensively shown to reduce to stable products, such as $Li_3N$, and contribute to LiF production in the SEI when paired with $TFSI^-$ in lithiated systems [36–40].

### 3.1. Differential scanning calorimetry

For traditional lithium-ion SPEs that use semicrystalline PEO, it is widely accepted that the primary ionic transport mechanism is coordination and subdiffusive motion of $Li^+$ along the polymer chain backbone, together with intersegmental hopping between polymer chains [41]. Therefore, if appreciable transport of $Li^+$ relies on segmental chain motion, a clear design goal for semicrystalline matrices is to improve ionic conductivity by suppressing crystallinity, thereby enhancing polymer chain mobility which facilitates ionic transport [42,43]. PAN's relatively high $T_g$ ~ 120 °C (Fig. S5A), the crossover temperature where polymer chains gain mobility, and lack of crystallinity suggest that $Li^+$ will exhibit ionic transport independent of polymer chain mobility. In fact, several studies suggest a nearly complete decoupling and establish a hierarchy of interactions for $Li^+$ that contribute to ionic conductivity: (1) movement of free $Li^+$ within the PAN matrix > (2) movement of $Li^+$ associated with plasticizer molecules > (3) movement of $Li^+$ due to coupling with PAN and segmental motion [44–46].

Along with the rational choice of PAN as the polymer matrix of interest, the compositions of the HAILSPE systems were carefully selected based on *a posteriori* knowledge of previous systems. Water concentration was allowed to range between 30—70 mol% since water is beneficial for transport properties but can be deleterious for electrochemical stability. LiTFSI was limited to a range of <30% mol% because it is a helpful plasticizer but can aggregate at high concentrations and negatively impact ionic conductivity. Ultimately, the systems were designed around a balance of solids (PAN, LiTFSI) and liquids (water, $S_{2,2,2}$/$Pyr_{1,3}$) to maintain a homogeneous and robust SPE.

The thermal properties of the four electrolytes were investigated via mDSC; their thermograms are given in Fig. 1. The compositions of the electrolytes used for mDSC analysis, after measuring final water content via TGA, are given in Table 1. mDSC was chosen over traditional DSC because of its increased accuracy and precision for measuring weak transitions or measuring multiple transitions occurring simultaneously

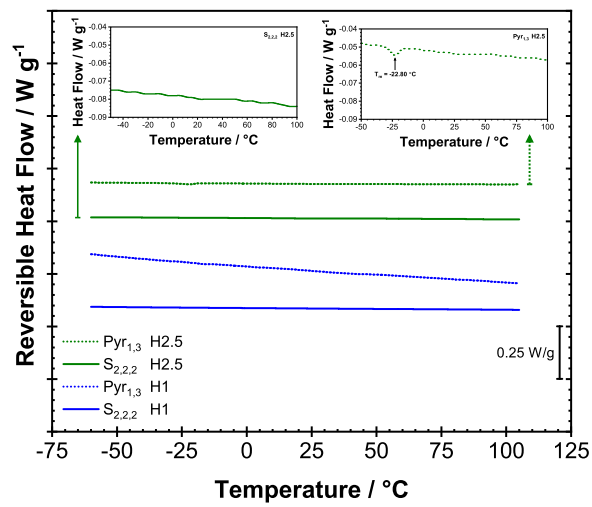


**Fig. 1.** mDSC thermograms (offset, exotherm up) in the heating direction over the range of -70 °C—110 °C for the four HAILSPE systems studied. The inset plots provide zoomed-in views of the (left) $S_{2,2,2}$ H2.5 and (right) $Pyr_{1,3}$ H2.5 electrolytes. The $Pyr_{1,3}$ H2.5 electrolyte shows a small, minimal melting transition at ~ -22.80 °C (0.725 J/g). A scalebar, representing 0.25 W/g, has been provided. The compositions of these electrolytes are provided in Table 1.

[47]. Furthermore, mDSC allows for measurement of the heat capacity and extraction of the reversible heat flow, which can better distinguish thermal responses based on heat capacity related transitions, such as $T_g$ or melting transition $T_m$. As observed in Fig. 1, each electrolyte exhibits a relatively flat thermal response, which indicates a suppression of crystallinity for the system. Both H1 electrolytes and $S_{2,2,2}$ H2.5 show zero crystallinity, while $Pyr_{1,3}$ H2.5 exhibits a small $T_m$ at ~ -22.80 °C. The enthalpy of this transition, found from the area under the curve, is only ~ 0.73 J/g, which is relatively insignificant compared to the total latent heat of each of the components (Fig. S5). While $Pyr_{1,3}$ H1 has 16.7% less water than $Pyr_{1,3}$ H2.5, no $T_m$ is observed in Fig. 1. Furthermore, $S_{2,2,2}$ H2.5 has a similar water content as $Pyr_{1,3}$ H2.5 (<1% difference), yet no transitions are observed. This suggests that the $T_m$ in $Pyr_{1,3}$ H2.5 is likely due to a combination of the increased water content, the highest of all four electrolytes studied, and the choice of ionic liquid. The increased ionic liquid content in $Pyr_{1,3}$ H2.5 compared to $Pyr_{1,3}$ H1 may help to plasticize the system and reduce the overall latent heat of the $T_m$ [19]. Nevertheless, because only one $T_m$ is observed at a relatively low temperature, lower than the expected operating conditions >0 °C, the system can be considered homogeneously well mixed with a minimal enough degree of crystallinity to still warrant further investigation.

### 3.2. Electrochemical impedance spectroscopy

To assess ionic mobility in the four HAILSPE systems, EIS was used to measure electrolyte resistance. Representative Nyquist plots are given in Fig. S6. From the ohmic resistance, *R*, ionic conductivity, in units of mS/cm, was calculated by

$$\sigma = 1000\frac{t}{R*A} \tag{4}$$

where $t$ and $A$ are the thickness and area of the electrolyte in units of cm and $cm^2$, respectively, as defined by the PTFE spacer. After analysis and data correction following the procedure outlined in the Supplemental Information, the Nyquist plots for each electrolyte system showed pure ionic conductor behavior at all temperatures. A simple equivalent circuit model with only one resistor was used to find the electrolyte resistance from the intercept of the data with the real impedance at high frequencies. This value is representative of the system's ohmic resistance, which includes losses due to the electrolyte, wires, and electric contacts (Fig. S7) [48].

The ionic conductivity values for the four electrolyte systems, over a range of temperatures from 0 to 80 °C in increments of 5 °C, are given in Fig. 2 and largely demonstrate the impact of water on the transport properties of these HAILSPEs. The compositions of the electrolytes used for EIS analysis are given in Table 1. While the electrolytes were designed with a specific intended amount of water to facilitate comparison, the extremely hygroscopic nature of the systems made it difficult to control the water absorption during processing in ambient conditions. As such, $Pyr_{1,3}$ H1 has ~ 63% more water than $S_{2,2,2}$ H1. This difference in water content results in a large discrepancy in ionic conductivity at all temperatures (e.g., 4.55 mS/cm and 2.31 mS/cm, respectively, at 25 °C), which is consistent with the results of similar systems that show ionic conductivity is heavily correlated with water concentration because of water's ability to coordinate with and solvate $Li^+$ [20,41]. The water content of $S_{2,2,2}$ H2.5 and $Pyr_{1,3}$ H2.5 was more precisely controlled, resulting in <1% difference. As a result, Fig. 2 shows that the ionic conductivity values more closely agree with one another than in the case of H1, particularly at low temperatures (≤30 °C). Furthermore, the water content of $Pyr_{1,3}$ H1 lies closer to $S_{2,2,2}$ and $Pyr_{1,3}$ H2.5 and shows comparable ionic conductivity values.

While Fig. 2 shows that increasing water content ($S_{2,2,2}$ H1 to $Pyr_{1,3}$ H1) leads to a notable improvement in mobility, the choice of ionic liquid and its impact on conductivity is not readily assessable. However, the linear behavior of these four HAILSPE systems with visually different slopes – especially $S_{2,2,2}$ H2.5 compared to $Pyr_{1,3}$ H2.5, which have nearly identical water content – suggests that there is, in fact, a dependency on the ionic liquid chemistry. To elucidate this effect, an Arrhenius regression was performed for the full-temperature ionic conductivity data, in the form of

$$\sigma = A*exp\left(\frac{-E_a}{RT}\right) \tag{5}$$

where $A$ is the pre-exponential factor and $E_a$ is the apparent activation energy. If Eq. (5) is linearized, then

$$\ln\sigma = \ln A - \frac{E_a}{R}\cdot\frac{1}{T} \tag{6}$$

which is in the form of $y = mx + b$. If $\ln\sigma$ is plotted as a function of inverse temperature, then the slope is $-\frac{E_a}{R}$ and the y-intercept is $\ln A$. For comparison, regression of the data to the classic Vogel-Tammann-Fulcher (VTF) equation for solid polymer electrolytes was performed and is presented in the Supplemental Information [49].

The linearized data for each of the four HAILSPE systems is presented in Fig. 3. Based on Eq. (6), $E_a$ and $\ln A$ were calculated from the slopes and y-intercepts of the fit lines, respectively. A summary of these values, including the $R^2$ fit parameter, is presented in Table 1. In SPE systems, $E_a$ is often regarded as contribution to ionic conductivity from the segmental motion of the polymer matrix while $A$ is thought to be related to the charge carrier concentration [49,50]. Thus, a lower $E_a$ would indicate further decoupling of ionic transport from polymer chain mobility. Fig. 3A and 3B present the Arrhenius fit for $S_{2,2,2}$ and $Pyr_{1,3}$ H1, respectively, while Fig. 3C and 3D present the Arrhenius fit for $S_{2,2,2}$ and $Pyr_{1,3}$ H2.5, respectively. When there is a large disparity in water content, as in $S_{2,2,2}$ vs $Pyr_{1,3}$ H1, $E_a$ remains constant – 0.307 eV and 0.302 eV, respectively – and no apparent trend is discernable. However, when water content is more carefully controlled, Fig. 3 suggests that both $E_a$ and $\ln A$ increase when changing the ionic liquid chemistry from $S_{2,2,2}$ – 0.243 eV and 4.11, respectively – to $Pyr_{1,3}$ – 0.292 eV and 6.14, respectively. Fig. 3 also suggests that the H2.5 composition yields lower activation energies, likely due to the increased amount of ionic liquid in the electrolyte that further plasticizes the polymer matrix to decouple ionic transport from polymer chain mobility. However, the purpose of this study was to investigate the effect of ionic liquid chemistry; the influence of modifying electrolyte composition will be investigated and reported elsewhere in a future publication.

While it is possible that the difference in $E_a$ from changing ionic liquid chemistry is due to an underlying fundamental phenomenon, studies indicate that $E_a$ can cover a wide range for most systems, rather than existing as a single value [51]. Nevertheless, the $E_a$ found in this work for each of the four HAILSPE systems is more comparable with liquid-phase electrolytes than SPEs. For example, activation energies of 0.259 eV and 0.275 eV were calculated for DME and DMSO organic electrolytes, respectively, under conditions where $Li^+$ were fully solvated [52]. In an EC + DEC organic electrolyte where $Li^+$ were completely nonsolvated, $E_a$ was significantly higher at ~ 0.583 eV. Aqueous electrolytes demonstrated similar $E_a$ values to the fully solvated organic electrolytes. The WiSE was found to have an estimated $E_a$ of ~ 0.286 eV, calculated from approximations based on the available conductivity data, which is comparable to $S_{2,2,2}$ H1, $Pyr_{1,3}$ H1, and $Pyr_{1,3}$ H2.5. The HANE was found to have an estimated $E_a$ of ~ 0.228 eV that is comparable to $S_{2,2,2}$ H2.5 [24,27]. In these liquid electrolytes, $E_a$ is thought to be related to the reorientation of interacting species rather than polymer segmental motion [53].

Based on Eq. (5), a general design principle can be developed to improve ionic conductivity by decreasing $E_a$ or increasing $A$. This principle, however, is predicated on the assumption that the underlying processes described are entirely different and completely uncorrelated. Many researchers have investigated the validity of this assumption and highlighted the importance of assessing the correlation between $E_a$ and

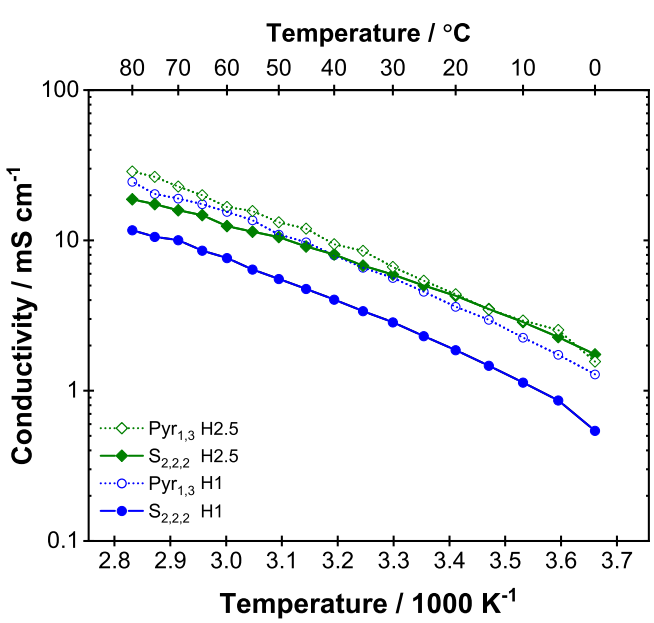


**Fig. 2.** Ionic conductivity, as measured by EIS over the temperature range of 0—80 °C in increments of 5 °C, of the HAILSPE compositions H1 (blue, circles) and H2.5 (green, diamonds) using $S_{2,2,2}$ (filled, solid line) and $Pyr_{1,3}$ (empty, dotted line) ionic liquids. $S_{2,2,2}$ H1 and $Pyr_{1,3}$ H1 have different water amounts, while $S_{2,2,2}$ H2.5 and $Pyr_{1,3}$ H2.5 have similar water amounts. The compositions of these electrolytes are provided in Table 1.

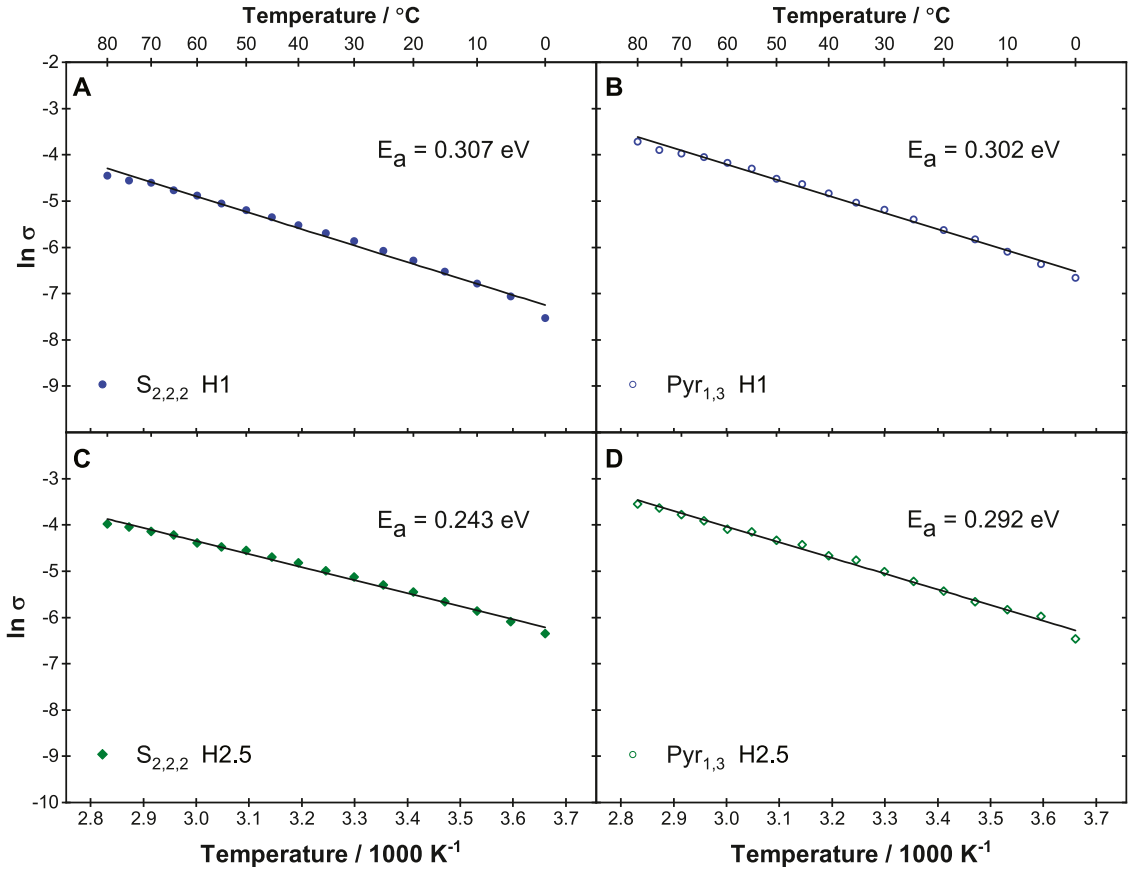


**Fig. 3.** Arrhenius plots of ionic conductivity for the four HAILSPE systems. (A) $S_{2,2,2}$ H1, (B) $Pyr_{1,3}$ H1, (C) $S_{2,2,2}$ H2.5, and (D) $Pyr_{1,3}$ H2.5. The apparent activation energies, calculated from the slope of the fit line, are provided for each electrolyte in units of eV. The compositions of these electrolytes are provided in Table 1, as well as the intercept of the fit line (ln*A*), the apparent activation energy in units of kJ/mol, and the $R^2$ value for the fit line.

*A* [50,53]. When a negative correlation between the two parameters exists, then the design principle remains unchanged. If, however, a positive correlation exists, the maximum ionic conductivity for a system corresponds to a minimized *A*. This realization is contradictory to the strategy employed for most aqueous electrolytes where the total number of charge carriers is increased to improve electrochemical stability [23,27,54–56]. To assess the degree of correlation for the HAILSPE systems reported here, ln*A* vs $E_a$ was plotted in Fig. 4 for the four electrolytes based on the values extracted from the Arrhenius regressions presented in Fig. 3 and summarized in Table 1. For comparison, the ln*A* and $E_a$

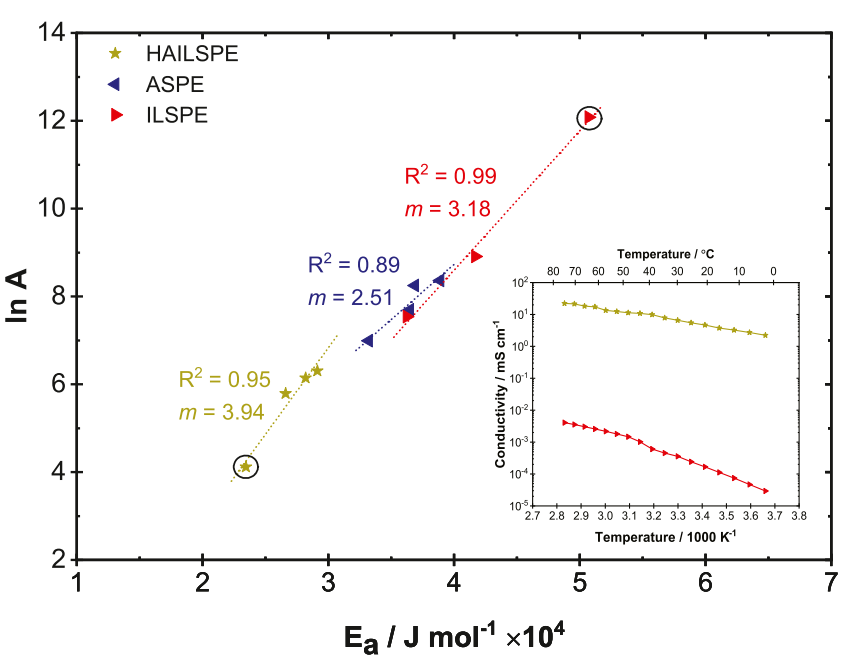


**Fig. 4.** Comparison of the correlation between the Arrhenius pre-exponential factor ln*A* and the apparent activation energy $E_a$ for the HAILSPE systems studied in this work (gold, stars) and previously studied ASPE (blue, left triangles) and ILSPE (red, right triangles) systems [19,20]. The slope *m* and $R^2$ value of the fit line for each set of electrolyte systems are provided. The inset plot shows the full-temperature ionic conductivity profiles for the circled electrolytes with the smallest ($S_{2,2,2}$ H2.5) and largest (ILSPE 3) $E_a$. The compositions of these electrolytes are provided in Tables 1, S1, and S2.

values were extracted for our previously reported ASPE and ILSPE systems (Table S1 and Table S2) that influenced the design of the HAILSPE systems [19,20].

Fig. 4 clearly shows that the HAILSPEs have the lowest apparent activation energies of the three systems, ranging from 23.45 kJ/mol to 29.60 kJ/mol. Compared to the ASPEs (33.23—38.91 kJ/mol) and ILSPEs (36.23—50.71 kJ/mol), this reduction in $E_a$ can be primarily attributed to the choice of PAN as the polymer matrix instead of PEO, where polymer chain mobility is a major contributor to ionic transport. In PAN-LiTFSI polymer-in-salt electrolytes, which are not plasticized by water or ionic liquid, of similar PAN:LiTFSI molar ratios used in the H1 and H2.5 systems, apparent activation energies of 33.32 kJ/mol were reported [57]. This value is comparable to even the well plasticized ASPE system with the lowest activation energy, indicating the large degree of decoupling provided by switching to PAN. Further reduction of the activation energies for the H1 and H2.5 systems can be attributed to the inclusion of water and IL that help plasticize the polymer matrix and offer additional decoupling of ionic conductivity from polymer chain mobility. The trend in ln$A$ in Fig. 4 is also consistent with the reduction of overall concentration of $Li^+$ from ~ 17.9—31.4 m in ASPE systems to ~ 4.4—10.4 m in HAILSPE systems when assuming water and ionic liquid as the only solvents.

From Fig. 4, a positive correlation between $E_a$ and $A$ is observed for each of the three studied systems, with the HAILSPEs ($R^2 = 0.95$) situated between the ILSPE ($R^2 = 0.99$) and ASPE ($R^2 = 0.89$) systems. As with the Arrhenius regression conducted in Fig. 3, the relationship between ln$A$ and $E_a$ in Fig. 4 can be described by the linear equation $\ln(\ln A) = mE_a + b$. From rearrangement of Eq. (6) and substitution of the linear equation, the relationship between the conductivities of two different electrolytes can be described by

$$\frac{\sigma_2}{\sigma_1} = \left(\frac{A_2}{A_1}\right)^{1-\left(\frac{1}{mRT}\right)} \tag{7}$$

which demonstrates that the change in ionic conductivity as a response to a change in $A$ is dependent on the value of $mRT$. If $mRT \geq 1$, then ionic conductivity is proportional to $A$ and increases with increasing $A$. If, however, $0 \leq mRT < 1$, then ionic conductivity is inversely proportional to $A$ and increases with decreasing $A$ [50]. Based on the slopes of the fit lines shown in Fig. 4, $mRT < 1$ for all three of the systems at room temperature, indicating that a decrease in $A$ causes an increase in ionic conductivity. Fig. 4 and the conductivity values given in Tables 1, S1, and S2 corroborate this result; HAILSPEs show the lowest value of ln$A$ (4.11), yet, on average, exhibit ionic conductivities ~ 4 orders of magnitude greater than the ILSPE composition with the highest value of ln$A$ (Fig. 4, inset). This outcome can be attributed to the design of the HAILSPE systems, which include both water and ionic liquid as plasticizers rather than each individually. While the inclusion of ionic liquid can artificially inflate the ionic conductivity due to the contribution from the cation, the room temperature lithium-specific conductivity $\sigma_{Li^+}$ – calculated by $t_{Li^+} \times \sigma_{25^\circ C}$ – given in Table 2 remains greater for all four HAILSPE systems than the four ASPE systems previously reported. The determination of $t_{Li^+}$, the transport number for $Li^+$, is discussed below.

### 3.3. pfg-NMR

To further investigate transport properties, pfg-NMR measurements were taken for the four HAILSPEs. The compositions of the electrolytes used for pfg-NMR analysis, after measuring final water content via TGA, are given in Table 2. Diffusion coefficients for $H_2O$ ($^1H$), $Li^+$ ($^7Li$), $IL^+$ ($S^+_{2,2,2}/Pyr^+_{1,3}$; $^1H$), and $TFSI^-$ ($^{19}F$) are plotted in Fig. 5 as a function of the lithium-ion mole fraction. For all compositions, $H_2O$ (squares) is the predominantly mobile species based on its diffusion coefficient. For the ions in the system, the diffusion coefficients follow the same order for all electrolytes: $Li^+$ (stars) > $IL^+$ (up triangles) > $TFSI^-$ (down triangles). For both $S_{2,2,2}$ H2.5 (green, solid) and $Pyr_{1,3}$ H2.5 (green, empty), $D_{H_2O}$ in Fig. 5 – and to a smaller degree, $D_{IL^+}$ – is likely overestimated because the parafilm wrapping used to prepare the samples is a saturated polyolefin that produces a background signal in the $^1H$ spectrum. When unsaturated PTFE was used to prepare samples for $S_{2,2,2}$ H1 (blue, solid) and $Pyr_{1,3}$ H1 (blue, empty), the background signal was significantly reduced and $D_{H_2O}$ and $D_{IL^+}$ more closely resemble $D_{Li^+}$ and $D_{TFSI^-}$ in Fig. 5.

In nonaqueous SPEs, $t_{Li^+}$ is readily measured using the Bruce-Vincent (BV) method to determine approximately what portion of the ionic conductivity can be attributed to the movement of $Li^+$ [19,58]. This technique, however, requires the use of lithium-metal electrodes and is therefore not compatible with aqueous electrolytes. Instead, an analogous transport number can be calculated from the diffusion coefficients obtained through pfg-NMR, given in Table 2, by

$$t_{Li^+} = \frac{c_{Li^+} * D_{Li^+}}{(c_{Li^+} * D_{Li^+}) + (c_{TFSI^-} * D_{TFSI^-}) + (c_{IL^+} * D_{IL^+})} \tag{8}$$

where $c_{Li^+}$ is the concentration of $Li^+$, $c_{TFSI^-}$ is the concentration of $TFSI^-$,

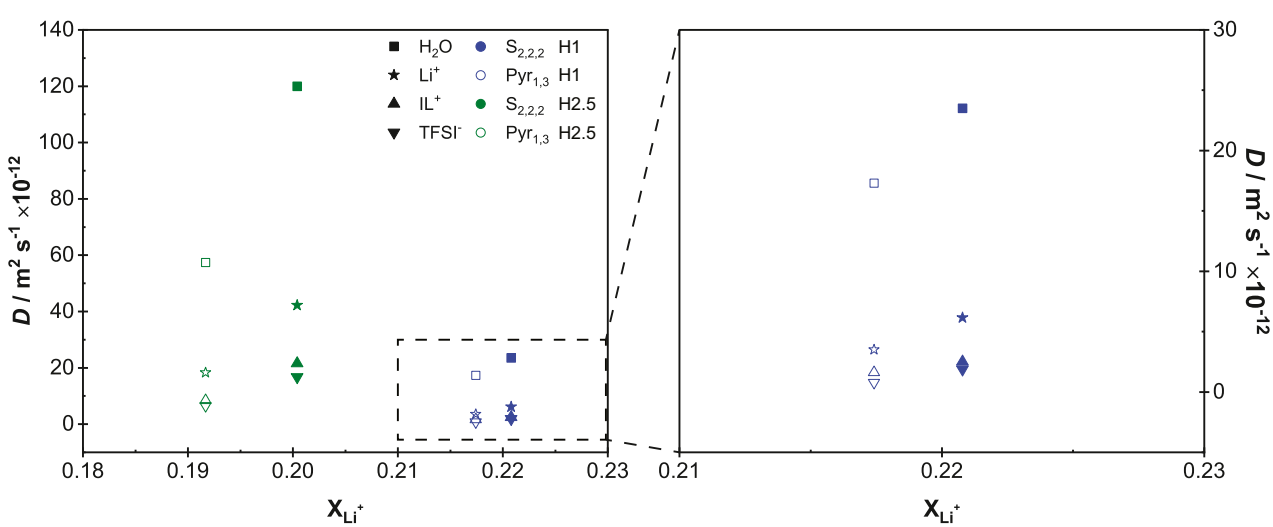


**Fig. 5.** pfg-NMR measured diffusion coefficients for the mobile species $H_2O$ (squares), $Li^+$ (stars), $IL^+$ (up triangles), and $TFSI^-$ (down triangles) present in $S_{2,2,2}$ H1 (blue, filled), $Pyr_{1,3}$ H1 (blue, empty), $S_{2,2,2}$ H2.5 (green, filled), and $Pyr_{1,3}$ H2.5 (green, empty) electrolytes expressed as a function of the lithium-ion mole fraction $X_{Li^+}$. The compositions of these electrolytes and the diffusion coefficients are given in Table 2.

**Table 2**
Summary of the properties determined from pfg-NMR measurements for the four HAILSPE systems investigated. The compositions of the electrolytes are provided and represent molar ratios. The room temperature lithium-ion conductivity was calculated by $\sigma_{Li^+_{25^\circ C}} = t_{Li^+} \times \sigma_{25^\circ C}$ using the ionic conductivity values given in Table 1.

| | PAN | $H_2O$ | IL | LiTFSI | $D_{Li^+}$ $\times 10^{-12}$ m$^2$ s$^{-1}$ | $D_{IL^+}$ $\times 10^{-12}$ m$^2$ s$^{-1}$ | $D_{TFSI^-}$ $\times 10^{-12}$ m$^2$ s$^{-1}$ | $t_{Li^+}$ | $\sigma_{Li^+_{25^\circ C}}$ mS cm$^{-1}$ |
|---|---|---|---|---|---|---|---|---|---|
| **$S_{2,2,2}$ H1** | 6.14 | 17.30 | 1 | 6.93 | 6.16 | 2.51 | 1.88 | 0.71 | 1.64 |
| **$Pyr_{1,3}$ H1** | 6.14 | 17.79 | 1 | 6.93 | 3.50 | 1.62 | 0.793 | 0.75 | 3.41 |
| **$S_{2,2,2}$ H2.5** | 6.14 | 19.00 | 2.5 | 6.93 | 42.2 | 21.6 | 16.7 | 0.58 | 2.91 |
| **$Pyr_{1,3}$ H2.5** | 6.14 | 20.57 | 2.5 | 6.93 | 18.3 | 8.46 | 6.57 | 0.60 | 3.23 |

and $c_{IL^+}$ is the ionic liquid cation ($S^+_{2,2,2}$ / $Pyr^+_{1,3}$) concentration. The transport numbers calculated from Eq. (8) are given in Table 2. The H1 electrolytes exhibited greater transport numbers (0.71, 0.75) at room temperature than the H2.5 electrolytes (0.58, 0.60). This is because the H2.5 systems contain more ionic liquid than the H1 systems, with relatively comparable amounts of polymer, water, and salt, which reduces the concentration of $Li^+$ and decreases $t_{Li^+}$. Furthermore, the electrolytes with $Pyr_{1,3}$ show greater transport numbers (0.75, 0.60) than the $S_{2,2,2}$ versions (0.71, 0.58), which may be due to self-aggregation of $Pyr_{1,3}$ into slower surfactant-like moieties that would reduce $Li^+$–$Pyr_{1,3}$ interactions in favor of interactions with more mobile water molecules [59]. This speculation agrees with the measured $D_{IL^+}$ values, which are 1.55—2.55 times smaller for the $Pyr_{1,3}$ electrolytes when compared to their $S_{2,2,2}$ analogs.

The pfg-NMR results presented in Fig. 5 and Table 2 are significant because they indicate a large degree of decoupling of ionic transport from polymer chain mobility, as predicted, and preferential $Li^+$ transport. If there was coupling, $IL^+$ and $TFSI^-$ would be largely unhindered and have higher diffusion coefficients relative to $Li^+$, resulting in significantly lower transport numbers ~0.2—0.4 often seen in SPEs [60]. For example, our previously reported ILSPE system, used for comparison in Fig. 4, exhibited $t_{Li^+}$ values in the range of 0.25—0.35 when measured using the BV method (Table S4) [19]. However, our previously reported ASPE system, also used for comparison in Fig. 4, exhibited $t_{Li^+}$ values comparable to the HAILSPE systems reported here, in the range of 0.64—0.67 (Table S3) [20]. It is interesting to note that the diffusion coefficients of the HAILSPE systems given in Table 2 are approximately the same as the diffusion coefficients for the ASPE systems in Table S3, also measured with pfg-NMR, yet the room temperature ionic conductivities for HAILSPE systems, given in Table 1, are 1.3—7.9 times greater. As discussed above, despite the ionic liquids contributing to total ionic conductivity, the room temperature $\sigma_{Li^+}$ is still greater for the HAILSPEs compared to the ASPEs. The diffusion coefficients may offer some insight, which show that the ratio of $D_{Li^+}$ to $D_{TFSI^-}$ is ~ 3 for HAILSPEs and ~ 2 for ASPEs, suggesting that the $TFSI^-$ are significantly slower in HAILSPEs, enabling $Li^+$ to move relatively faster. Furthermore, this suggests that the transport of $Li^+$ is further decoupled from polymer chain mobility, which can also account for the improvement in conductivity [61].

### 3.4. Linear sweep and cyclic voltammetry

As discussed previously, PAN was selected because of its reported strong oxidative stability [62]. To further understand the oxidative stability of HAILSPE systems, LSV was used to assess the anodic limit of the electrolytes. Fig. 6A and 6B show the representative current density of both H1 and H2.5 systems, respectively, as a function of cell potential. For all systems, the same trend was observed: generally low current evolution starting at ~ 4.2 V vs. $Li/Li^+$, likely due to minor oxidation of PAN, followed by rapid current evolution at potentials >5.4 V vs. $Li/Li^+$ due to complete electrolyte degradation. While it is difficult to accurately assess the electrochemical stability window in SPEs, this result supports the generally favorable oxidative stability of PAN-based electrolytes [63,64].

To assess cathodic stability, CV was used to monitor the passivating behavior and SEI formation in each of the four HAILSPE systems. A modest limit of ~ 2 V vs. $Li/Li^+$ was chosen to investigate this behavior without causing irreversible electrolyte degradation. Figs. 7 and 8 display the first 5 cycles for H1 and H2.5 electrolytes, respectively. The current response at low potentials is due to $H_2O$ reduction, thus it is expected that systems with more water will yield larger current densities. The results for $Pyr_{1,3}$ H1 and $Pyr_{1,3}$ H2.5 support this claim; in Fig. 8B, $Pyr_{1,3}$ H2.5 contained ~ 3 times as much water and measured a current density ~ 2 times greater than the $Pyr_{1,3}$ H1 electrolyte at the

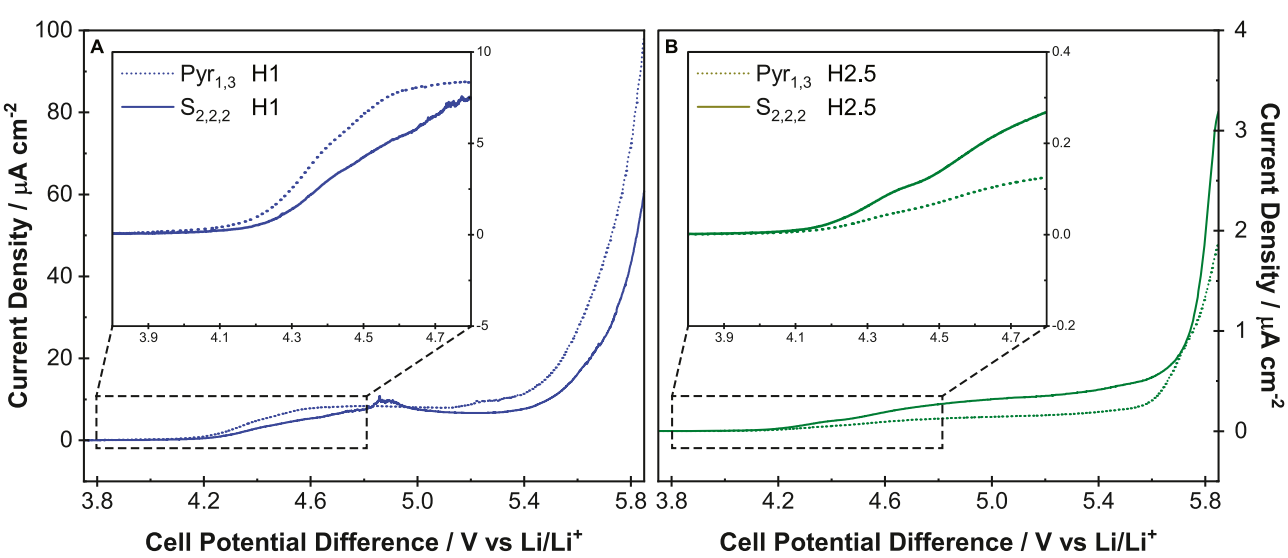


**Fig. 6.** Determination of the anodic limit via LSV from current density as a function of cell potential for the (A) $S_{2,2,2}$ (blue, solid) and $Pyr_{1,3}$ (blue, dashed) H1 electrolytes, and (B) $S_{2,2,2}$ (green, solid) and $Pyr_{1,3}$ (green, dashed) H2.5 electrolytes. Insets provide a zoomed-in view limited to 10% of the ordinate over the range of 3.8—4.8 V vs. $Li/Li^+$. All electrolytes were measured at room temperature with a scan rate of 0.5 mV/s.

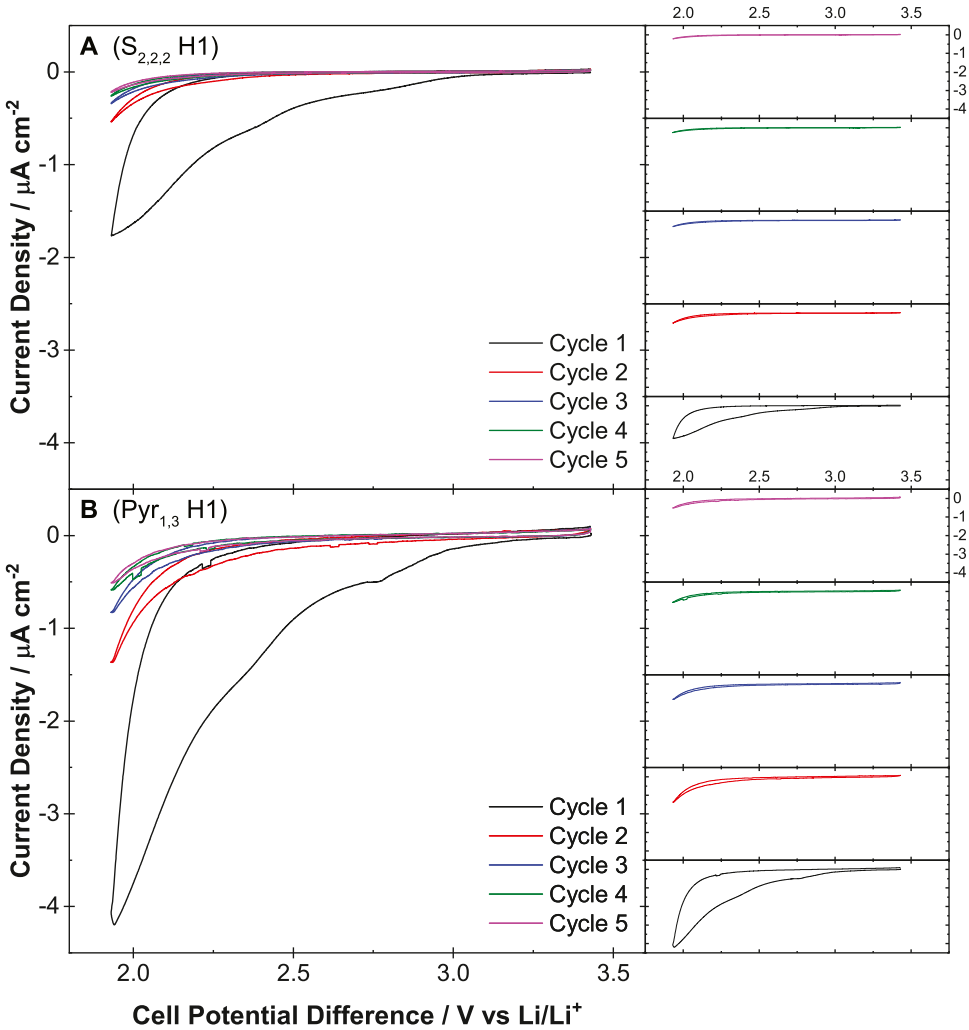


**Fig. 7.** CV measured passivation given by current density as a function of cell potential, limited to 2 V vs. $Li/Li^+$, for (A) $S_{2,2,2}$ H1 and (B) $Pyr_{1,3}$ H1. The first 5 cycles are presented in both overlayed and stacked forms. $S_{2,2,2}$ H1 had a final water molar ratio of 9.40 and $Pyr_{1,3}$ H1 had a final water molar ratio of 7.24. All electrolytes were measured at room temperature with a scan rate of 0.5 mV/s.

selected limit shown in Fig. 7B. Furthermore, it is immediately clear from Figs. 7 and 8 that for both systems, the $Pyr_{1,3}$ version yields a larger current density in the first cycle than the $S_{2,2,2}$ version. This finding aligns with pfg-NMR results that suggested $Pyr_{1,3}$ systems had reduced $Li^+$–$Pyr^+_{1,3}$ interactions in favor of interactions with water. Increased $Li^+$–$H_2O$ interactions are expected to lead to a higher concentration of water available for reduction as lithium ions shuttle water to the anode surface.

Figs. 7 and 8 also provide information regarding the quality of the SEI formed during passivation at the selected limit. Trends in successive cycles can indicate one of two main pathways for SEI growth: tunnelling or self-inhibition. In the first case, the SEI is uniform but thin enough to allow electron tunnelling through it. Thus, current evolution indicates an increase in SEI thickness [65]. In CV measurements, tunnelling is represented by a shift in the potential of the reduction peak with consecutive cycling. In the more common second case, the SEI is non-uniform but thick enough to block electron tunnelling through it. Thus, current evolution indicates additional SEI formation at unblocked sites and improves coverage. In CV measurements, self-inhibition is represented by a decrease in the current density with consecutive cycling [65,66]. The decrease in current density observed over consecutive cycles in Figs. 7 and 8 clearly indicates a self-inhibitory pathway of SEI growth for both H1 and H2.5 systems. Furthermore, the CV results suggest that growth of the thick SEI is relatively fast and completes with full surface coverage within the first 5 cycles, as evidenced by the drastic decrease in current density after the first full cycle in all cases.

## 4. Conclusion

To improve the cathodic limit of aqueous electrolytes, new design strategies are essential. The recent development of HANE systems shows a promising step forward, yet these electrolytes often sacrifice transport properties to improve reductive stability. HAILSPEs characterized in this work provide an alternative pathway to these aqueous systems for solid-state analogs, demonstrating a strategy to tune the degree of passivation at the anode while simultaneously improving transport properties. $Pyr_{1,3}$ H2.5 exhibited a room temperature ionic conductivity of 5.39 mS/cm, 3 times greater than even the most conductive ASPE predecessor. This same electrolyte, however, exhibited the largest degree of $H_2O$ reduction before complete passivation, reaching a peak current density of $\sim 9$ μA/cm$^2$. When the electrolyte composition is modified slightly, the peak current density of $Pyr_{1,3}$ H1 is limited to $\sim 4$ μA/cm$^2$. Switching the ionic liquid chemistry even further reduces the peak current density to $<2$ μA/cm$^2$ for $S_{2,2,2}$ H1, however this electrolyte maintains an ionic conductivity less than half of $Pyr_{1,3}$ H2.5. These results clearly show a continued tradeoff between transport properties and passivation, highlighting the need for optimization before assessing performance in Li-ion battery systems. Nevertheless, the HAILSPE systems still displayed

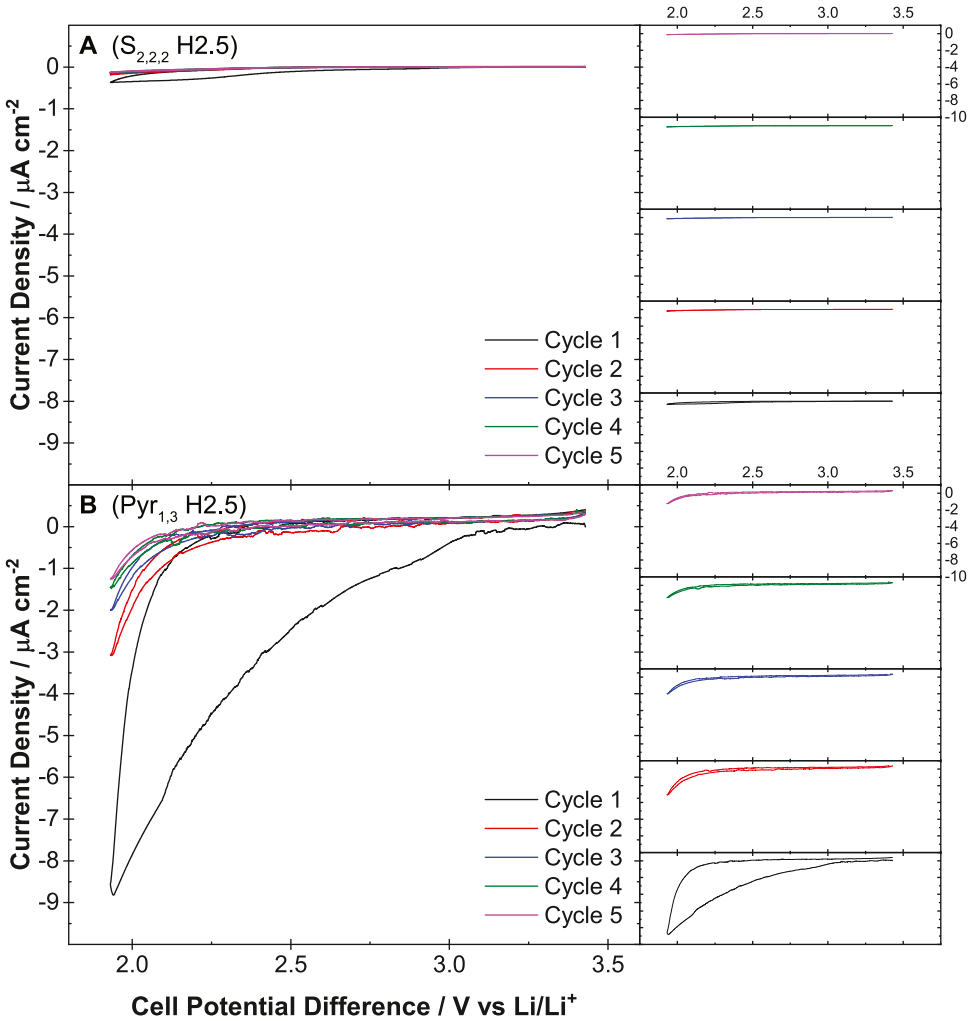


**Fig. 8.** CV measured passivation given by current density as a function of cell potential, limited to 2 V vs. Li/Li$^+$, for (A) $S_{2,2,2}$ H2.5 and (B) $Pyr_{1,3}$ H2.5. The first 5 cycles are presented in both overlayed and stacked forms. $S_{2,2,2}$ H2.5 had a final water molar ratio of 30.55 and $Pyr_{1,3}$ H2.5 had a final water molar ratio of 30.91. All electrolytes were measured at room temperature with a scan rate of 0.5 mV/s.

remarkable improvement of transport properties from their ASPE predecessors while demonstrating the capability to tune the degree of passivation. This precursory work, whose goal was to determine the fundamental properties of HAILSPEs as they relate to transport and passivation, will help to guide future efforts and provide a route forward for aqueous SPEs.

## CRediT authorship contribution statement

**Kyle B. Ludwig:** Conceptualization, Methodology, Validation, Formal analysis, Investigation, Data curation, Writing – original draft, Writing – review & editing, Visualization. **Riordan Correll-Brown:** Formal analysis, Investigation, Data curation, Writing – review & editing, Visualization. **Max Freidlin:** Formal analysis, Investigation, Data curation. **Mounesha N. Garaga:** Methodology, Formal analysis, Investigation. **Sahana Bhattacharyya:** Formal analysis, Investigation. **Patricia M. Gonzales:** Formal analysis, Investigation. **Arthur V. Cresce:** Resources, Supervision. **Steve Greenbaum:** Resources, Supervision. **Chunsheng Wang:** Supervision. **Peter Kofinas:** Conceptualization, Resources, Writing – review & editing, Supervision, Project administration, Funding acquisition.

## Declaration of Competing Interest

The authors declare that they have no known competing financial interests or personal relationships that could have appeared to influence the work reported in this paper.

## Acknowledgements

This work was supported by the National Science Foundation [grant number CBET2037835]; and the DEVCOM Army Research Laboratory [cooperative agreement number W911NF-22-2-0021]. The opinions, findings, views, conclusions, or recommendations expressed in this material are those of the authors and should not be interpreted as representing the official policies, either expressed or implied, of the Army Research Office, the National Science Foundation, or the U.S. Government. The U.S. Government is authorized to reproduce and distribute reprints for Government purposes notwithstanding any copyright notation herein.

The authors would like to express their gratitude to Dr. Mark Orazem for his invaluable insights and assistance in developing our error model analysis method. The authors are also grateful for the US Army Research Laboratory and the Battery Science Branch for use of their facilities and their continued spirit of governmental and academic collaboration. We thank Jesse Matthews, Olivier Izmery, and Sam Chen for their early efforts on this work and Jacob Sandler for his efforts on the EIS analysis.

## Supplementary materials

Supplementary material associated with this article can be found, in the online version, at doi:10.1016/j.electacta.2023.142349.

## References


[1] M. Li, J. Lu, Z. Chen, K. Amine, 30 years of lithium-ion batteries, Adv. Mater. 30 (2018), 1800561, https://doi.org/10.1002/ADMA.201800561.

[2] M.v. Reddy, A. Mauger, C.M. Julien, A. Paolella, K. Zaghib, Brief history of early lithium-battery development, Materials (2020) 13, https://doi.org/10.3390/MA13081884.

[3] J.B. Goodenough, K.S. Park, The Li-ion rechargeable battery: a perspective, J. Am. Chem. Soc. 135 (2013) 1167–1176, https://doi.org/10.1021/JA3091438/ASSET/IMAGES/JA-2012-091438_M014.GIF.

[4] B. Dunn, H. Kamath, J.M. Tarascon, Electrical energy storage for the grid: a battery of choices, Science 334 (2011) 928–935, https://doi.org/10.1126/SCIENCE.1212741/SUPPL_FILE/DUNN-SOM.PDF (1979).

[5] T. Kim, W. Song, D.Y. Son, L.K. Ono, Y. Qi, Lithium-ion batteries: outlook on present, future, and hybridized technologies, J. Mater Chem. A Mater. 7 (2019) 2942–2964, https://doi.org/10.1039/C8TA10513H.

[6] L. Lu, X. Han, J. Li, J. Hua, M. Ouyang, A review on the key issues for lithium-ion battery management in electric vehicles, J. Power Sources 226 (2013) 272–288, https://doi.org/10.1016/J.JPOWSOUR.2012.10.060.

[7] J.B. Goodenough, Y. Kim, Challenges for rechargeable Li batteries, Chem. Mater. 22 (2010) 587–603, https://doi.org/10.1021/CM901452Z/ASSET/IMAGES/LARGE/CM-2009-01452Z_0018.JPEG.

[8] M. Armand, J.-M. Tarascon, Building better batteries, Nature 451 (2008) 652–657, https://doi.org/10.1038/451652a.

[9] B. Boz, T. Dev, A. Salvadori, J.L. Schaefer, Review—electrolyte and electrode designs for enhanced ion transport properties to enable high performance lithium batteries, J. Electrochem. Soc. 168 (2021), 090501, https://doi.org/10.1149/1945-7111/AC1CC3.

[10] N. Williard, W. He, C. Hendricks, M. Pecht, Lessons learned from the 787 Dreamliner issue on lithium-ion battery reliability, Energies 6 (2013) 4682–4695, https://doi.org/10.3390/en6094682 (Basel).

[11] J.M. Tarascon, M. Armand, Issues and challenges facing rechargeable lithium batteries, Nature 414 (6861) (2001) 359–367, https://doi.org/10.1038/35104644, 2001414.

[12] K. Xu, Electrolytes and interphases in Li-ion batteries and beyond, Chem. Rev. 114 (2014) 11503–11618, https://doi.org/10.1021/cr500003w.

[13] K. Xu, Nonaqueous liquid electrolytes for lithium-based rechargeable batteries, Chem. Rev. 104 (2004) 4303–4418, https://doi.org/10.1021/cr030203g.

[14] Q. Wang, L. Jiang, Y. Yu, J. Sun, Progress of enhancing the safety of lithium ion battery from the electrolyte aspect, Nano Energy 55 (2019) 93–114, https://doi.org/10.1016/j.nanoen.2018.10.035.

[15] L. Edman, M.M. Doeff, A. Ferry, J. Kerr, L.C. de Jonghe, Transport properties of the solid polymer electrolyte system P(EO)nLiTFSI, J. Phys. Chem. B 104 (2000) 3476–3480, https://doi.org/10.1021/jp993897z.

[16] K. Murata, S. Izuchi, Y. Yoshihisa, Overview of the research and development of solid polymer electrolyte batteries, Electrochim. Acta 45 (2000) 1501–1508, https://doi.org/10.1016/S0013-4686(99)00365-5.

[17] Y. Jiang, X. Yan, Z. Ma, P. Mei, W. Xiao, Q. You, Y. Zhang, Development of the PEO based solid polymer electrolytes for all-solid state lithium ion batteries, Polymers 10 (2018) 1237, https://doi.org/10.3390/polym10111237 (Basel).

[18] G.B. Appetecchi, J. Hassoun, B. Scrosati, F. Croce, F. Cassel, M. Salomon, Hot-pressed, solvent-free, nanocomposite, PEO-based electrolyte membranes, J. Power Sources 124 (2003) 246–253, https://doi.org/10.1016/S0378-7753(03)00611-6.

[19] M.D. Widstrom, K.B. Ludwig, J.E. Matthews, A. Jarry, M. Erdi, A.v. Cresce, G. Rubloff, P. Kofinas, Enabling high performance all-solid-state lithium metal batteries using solid polymer electrolytes plasticized with ionic liquid, Electrochim. Acta 345 (2020), 136156, https://doi.org/10.1016/j.electacta.2020.136156.

[20] M.D. Widstrom, O. Borodin, K.B. Ludwig, J.E. Matthews, S. Bhattacharyya, M. Garaga, A.v. Cresce, A. Jarry, M. Erdi, C. Wang, S. Greenbaum, P. Kofinas, Water domain enabled transport in polymer electrolytes for lithium-ion batteries, Macromolecules 54 (2021) 2882–2891, https://doi.org/10.1021/acs.macromol.0c01960.

[21] J.L. Schaefer, D.A. Yanga, L.A. Archer, High lithium transference number electrolytes via creation of 3-dimensional, charged, nanoporous networks from dense functionalized nanoparticle composites, Chem. Mater. 25 (2013) 834–839, https://doi.org/10.1021/CM303091J/ASSET/IMAGES/LARGE/CM-2012-03091J_0007.JPEG.

[22] C. Yang, J. Chen, T. Qing, X. Fan, W. Sun, A. von Cresce, M.S. Ding, O. Borodin, J. Vatamanu, M.A. Schroeder, N. Eidson, C. Wang, K. Xu, 4.0 V aqueous Li-ion batteries, Joule 1 (2017) 122–132, https://doi.org/10.1016/j.joule.2017.08.009.

[23] L. Suo, O. Borodin, W. Sun, X. Fan, C. Yang, F. Wang, T. Gao, Z. Ma, M. Schroeder, A. von Cresce, S.M. Russell, M. Armand, A. Angell, K. Xu, C. Wang, Advanced high-voltage aqueous lithium-ion battery enabled by "water-in-Bisalt" electrolyte, Angew. Chem. Int. Ed. 55 (2016) 7136–7141, https://doi.org/10.1002/ANIE.201602397.

[24] F. Wang, O. Borodin, M.S. Ding, M. Gobet, J. Vatamanu, X. Fan, T. Gao, N. Edison, Y. Liang, W. Sun, S. Greenbaum, K. Xu, C. Wang, Hybrid aqueous/non-aqueous electrolyte for safe and high-energy Li-ion batteries, Joule 2 (2018) 927–937.

[25] H. Zhang, B. Qin, J. Han, S. Passerini, Aqueous/nonaqueous hybrid electrolyte for sodium-ion batteries, ACS Energy Lett. 3 (2018) 1769–1770, https://doi.org/10.1021/acsenergylett.8b00919.

[26] J. Zhu, Y. Xu, Y. Fu, D. Xiao, Y. Li, L. Liu, Y. Wang, Q. Zhang, J. Li, X. Yan, J.J. Zhu, Y.T. Xu, L.Y. Liu, Q.N. Zhang, X.B. Yan, Y.J. Fu, Y.L. Li, Y. Wang, J.S. Li, D.W. Xiao, Hybrid aqueous/nonaqueous water-in-Bisalt electrolyte enables safe dual ion batteries, Small 16 (2020), 1905838, https://doi.org/10.1002/SMLL.201905838.

[27] L. Suo, O. Borodin, T. Gao, M. Olguin, J. Ho, X. Fan, C. Luo, C. Wang, K. Xu, Water-in-salt" electrolyte enables high-voltage aqueous lithium-ion chemistries, Science (1979) 350 (2015) 938–943, https://doi.org/10.1126/science.aab1595.

[28] E.O. Stejskal, J.E. Tanner, Spin diffusion measurements: Spin echoes in the presence of a time-dependent field gradient, J. Chem. Phys. 42 (1965) 288–292, https://doi.org/10.1063/1.1695690.

[29] H. Zhang, F. Chen, O. Lakuntza, U. Oteo, L. Qiao, M. Martinez-Ibañez, H. Zhu, J. Carrasco, M. Forsyth, M. Armand, Suppressed mobility of negative charges in polymer electrolytes with an ether-functionalized anion, Angew. Chem. Int. Ed. 58 (2019) 12070–12075, https://doi.org/10.1002/ANIE.201905794.

[30] P. Hu, J. Chai, Y. Duan, Z. Liu, G. Cui, L. Chen, Progress in nitrile-based polymer electrolytes for high performance lithium batteries, J. Mater Chem. A Mater. 4 (2016) 10070–10083, https://doi.org/10.1039/c6ta02907h.

[31] S. Panero, D. Satolli, A. D'Epifano, B. Scrosati, High voltage lithium polymer cells using a PAN-based composite electrolyte, J. Electrochem. Soc. 149 (2002) A414, https://doi.org/10.1149/1.1454139.

[32] J. Mindemark, M.J. Lacey, T. Bowden, D. Brandell, Beyond PEO—alternative host materials for Li+-conducting solid polymer electrolytes, Prog. Polym. Sci. 81 (2018) 114–143, https://doi.org/10.1016/j.progpolymsci.2017.12.004.

[33] O. Borodin, L. Suo, M. Gobet, X. Ren, F. Wang, A. Faraone, J. Peng, M. Olguin, M. Schroeder, M.S. Ding, E. Gobrogge, A. von Wald Cresce, S. Munoz, J.A. Dura, S. Greenbaum, C. Wang, K. Xu, Liquid structure with nano-heterogeneity promotes cationic transport in concentrated electrolytes, ACS Nano 11 (2017) 10462–10471, https://doi.org/10.1021/acsnano.7b05664.

[34] L. Suo, D. Oh, Y. Lin, Z. Zhuo, O. Borodin, T. Gao, F. Wang, A. Kushima, Z. Wang, H.C. Kim, Y. Qi, W. Yang, F. Pan, J. Li, K. Xu, C. Wang, How solid-electrolyte interphase forms in aqueous electrolytes, J. Am. Chem. Soc. 139 (2017) 18670–18680, https://doi.org/10.1021/jacs.7b10688.

[35] Y. Yamada, A. Yamada, Superconcentrated electrolytes to create new interfacial chemistry in non-aqueous and aqueous rechargeable batteries, Chem. Lett. 46 (2017) 1056–1064, https://doi.org/10.1246/cl.170284.

[36] A. Basile, A.I. Bhatt, A.P. O'Mullane, Stabilizing lithium metal using ionic liquids for long-lived batteries, Nat Commun 7 (2016), https://doi.org/10.1038/ncomms11794 ncomms11794.

[37] A. Budi, A. Basile, G. Opletal, A.F. Hollenkamp, A.S. Best, R.J. Rees, A.I. Bhatt, A. P. O'Mullane, S.P. Russo, Study of the initial stage of solid electrolyte interphase formation upon chemical reaction of lithium metal and N -methyl- N -propyl-pyrrolidinium- bis(fluorosulfonyl)imide, J. Phys. Chem. C 116 (2012) 19789–19797, https://doi.org/10.1021/jp304581g.

[38] J. Zheng, M. Gu, H. Chen, P. Meduri, M.H. Engelhard, J.G. Zhang, J. Liu, J. Xiao, Ionic liquid-enhanced solid state electrolyte interface (SEI) for lithium-sulfur batteries, J. Mater Chem. A Mater. 1 (2013) 8464–8470, https://doi.org/10.1039/c3ta11553d.

[39] H. Yoon, H. Zhu, A. Hervault, M. Armand, D.R. MacFarlane, M. Forsyth, Physicochemical properties of N-propyl-N-methylpyrrolidinium bis(fluorosulfonyl) imide for sodium metal battery applications, Phys. Chem. Chem. Phys. 16 (2014) 12350–12355, https://doi.org/10.1039/c4cp00365a.

[40] C.v. Manohar, M. Forsyth, D.R. MacFarlane, S. Mitra, Role of N-Propyl-N-Methyl Pyrrolidinium bis(trifluoromethanesulfonyl)imide as an electrolyte additive in sodium battery electrochemistry, Energy Technol. 6 (2018) 2232–2237, https://doi.org/10.1002/ente.201800123.

[41] O. Borodin, G.D. Smith, Mechanism of ion transport in amorphous poly(ethylene oxide)/LiTFSI from molecular dynamics simulations, Macromolecules 39 (2006) 1620–1629, https://doi.org/10.1021/ma052277v.

[42] Q. Zhao, S. Stalin, C.Z. Zhao, L.A. Archer, Designing solid-state electrolytes for safe, energy-dense batteries, Nat. Rev. Mater. 5 (2020) 229–252, https://doi.org/10.1038/s41578-019-0165-5.

[43] D.T. Hallinan, N.P. Balsara, Polymer electrolytes, Annu. Rev. Mater Res. 43 (2013) 503–525, https://doi.org/10.1146/ANNUREV-MATSCI-071312-121705/SUPPL_FILE/MR43_HALLINAN_SUPMAT.PDF.

[44] N. Voigt, L. van Wüllen, The mechanism of ionic transport in PAN-based solid polymer electrolytes, Solid State Ion 208 (2012) 8–16, https://doi.org/10.1016/j.ssi.2011.11.031.

[45] M. Watanabe, M. Kanba, K. Nagaoka, I. Shinohara, Ionic conductivity of hybrid films composed of polyacrylonitrile, ethylene carbonate, and $LiClO_4$, J. Polymer Sci. Part A-2 Polymer Phys. 21 (1983) 939–948, https://doi.org/10.1002/pol.1983.180210610.

[46] Z. Wang, B. Huang, R. Xue, X. Huang, L. Chen, Spectroscopic investigation of interactions among components and ion transport mechanism in polyacrylonitrile based electrolytes, Solid State Ion 121 (1999) 141–156, https://doi.org/10.1016/S0167-2738(98)00541-4.

[47] C. Leyva-Porras, P. Cruz-Alcantar, V. Espinosa-Solís, E. Martínez-Guerra, C. I. Piñón-Balderrama, I.C. Martínez, M.Z. Saavedra-Leos, Application of differential scanning calorimetry (DSC) and modulated differential scanning calorimetry (MDSC) in food and drug industries, Polymers 12 (2020) 5, https://doi.org/10.3390/POLYM12010005 (Basel).

[48] J. Rodríguez, S. Palmas, M. Sánchez-Molina, E. Amores, L. Mais, R. Campana, Simple and precise approach for determination of ohmic contribution of

diaphragms in alkaline water electrolysis, Membranes 9 (2019) 129, https://doi.org/10.3390/MEMBRANES9100129 (Basel).
[49] J.R. MacCallum, C.A. Vincent, Polymer Electrolyte Reviews, Springer, 1989.
[50] K.M. Diederichsen, H.G. Buss, B.D. McCloskey, The compensation effect in the Vogel-Tammann-Fulcher (VTF) equation for polymer-based electrolytes, Macromolecules 50 (2017) 3831–3840, https://doi.org/10.1021/ACS.MACROMOL.7B00423/ASSET/IMAGES/MA-2017-00423A_M006.GIF.
[51] A.S. Keefe, S. Buteua, I.G. Hill, J.R. Dahn, Temperature dependent EIS Studies separating charge transfer impedance from contact impedance in lithium-ion symmetric cells, J Electrochem. Soc. 166 (2019) A3272–A3279, https://doi.org/10.1149/2.0541914jes.
[52] T. Abe, H. Fukuda, Y. Iriyama, Z. Ogumi, Solvated Li-ion transfer at interface between graphite and electrolyte, J. Electrochem. Soc. 151 (2004) A1120–A1123, https://doi.org/10.1149/1.1763141.
[53] M. Petrowsky, R. Frech, Application of the compensated arrhenius formalism to self-diffusion: implications for ionic conductivity and dielectric relaxation, J. Phys. Chem. B 114 (2010) 8600–8605, https://doi.org/10.1021/JP1020142/SUPPL_FILE/JP1020142_SI_001.PDF.
[54] S. Ko, Y. Yamada, K. Miyazaki, T. Shimada, E. Watanabe, Y. Tateyama, T. Kamiya, T. Honda, J. Akikusa, A. Yamada, Lithium-salt monohydrate melt: a stable electrolyte for aqueous lithium-ion batteries, Electrochem. Commun. 104 (2019), 106488, https://doi.org/10.1016/J.ELECOM.2019.106488.
[55] L. Chen, J. Zhang, Q. Li, J. Vatamanu, X. Ji, T.P. Pollard, C. Cui, S. Hou, J. Chen, C. Yang, L. Ma, M.S. Ding, M. Garaga, S. Greenbaum, H.-S. Lee, O. Borodin, K. Xu, C. Wang, A 63 m superconcentrated aqueous electrolyte for high-energy Li-ion batteries, ACS Energy Lett. 5 (2020) 968–974, https://doi.org/10.1021/ACSENERGYLETT.0C00348.
[56] C. Yang, X. Ji, X. Fan, T. Gao, L. Suo, F. Wang, W. Sun, J. Chen, L. Chen, F. Han, L. Miao, K. Xu, K. Gerasopoulos, C. Wang, C. Yang, X. Ji, X. Fan, T. Gao, L. Suo, F. Wang, W. Sun, J. Chen, L. Chen, F. Han, C. Wang, L. Miao, K. Xu, K. Gerasopoulos, Flexible aqueous Li-ion battery with high energy and power densities, Adv. Mater. 29 (2017), 1701972, https://doi.org/10.1002/ADMA.201701972.
[57] B. Wu, L. Wang, Z. Li, M. Zhao, K. Chen, S. Liu, Y. Pu, J. Li, Performance of "polymer-in-salt" electrolyte PAN-LiTFSI enhanced by graphene oxide filler, J. Electrochem. Soc. 163 (2016) A2248–A2252, https://doi.org/10.1149/2.0531610JES/XML.
[58] J. Evans, C.A. Vincent, P.G. Bruce, Electrochemical measurement of transference numbers in polymer electrolytes, Polymer 28 (1987) 2324–2328, https://doi.org/10.1016/0032-3861(87)90394-6 (Guildf).
[59] M. Kunze, E. Paillard, S. Jeong, G.B. Appetecchi, M. Schönhoff, M. Winter, S. Passerini, Inhibition of self-aggregation in ionic liquid electrolytes for high-energy electrochemical devices, J. Phys. Chem. C 115 (2011) 19431–19436, https://doi.org/10.1021/jp2055969.
[60] M. Chiara Borghini, M. Mastragostino, S. Passerini, - al, S.C. Nunes, V. de Zea Bermudez, D. Ostrovskii, T. Mixtures Andrew Webber -, W. Goreckit, M. Jeannint, E. Belorizkyt, C. Roux, M. Armand, Physical properties of solid polymer electrolyte PEO(LiTFSI) complexes, J. Phys. Condens. Matter 7 (1995) 6823, https://doi.org/10.1088/0953-8984/7/34/007.
[61] H.O. Ford, B. Park, J. Jiang, M.E. Seidler, J.L. Schaefer, Enhanced Li+ conduction within single-ion conducting polymer gel electrolytes via reduced cation-polymer interaction, ACS Mater. Lett. 2 (2020) 272–279, https://doi.org/10.1021/ACSMATERIALSLETT.9B00510/ASSET/IMAGES/LARGE/TZ9B00510_0004.JPEG.
[62] C.F.N. Marchiori, R.P. Carvalho, M. Ebadi, D. Brandell, C.M. Araujo, Understanding the electrochemical stability window of polymer electrolytes in solid-state batteries from atomic-scale modeling: the role of Li-ion salts, Chem. Mater. 32 (2020) 7237–7246, https://doi.org/10.1021/ACS.CHEMMATER.0C01489/ASSET/IMAGES/LARGE/CM0C01489_0005.JPEG.
[63] A. Méry, S. Rousselot, D. Lepage, M. Dollé, A critical review for an accurate electrochemical stability window measurement of solid polymer and composite electrolytes, materials 14 (2021) 3840, https://doi.org/10.3390/MA14143840, 2021, Vol. 14, Page 3840.
[64] D.T. Hallinan, A. Rausch, B. McGill, An electrochemical approach to measuring oxidative stability of solid polymer electrolytes for lithium batteries, Chem. Eng. Sci. 154 (2016) 34–41, https://doi.org/10.1016/J.CES.2016.06.054.
[65] H.G. Steinrück, Modeling cyclic voltammetry during solid electrolyte interphase formation: baseline scenario of a dynamically evolving tunneling barrier resulting from a homogeneous single-phase insulating film, J. Chem. Phys. 154 (2021), 174703, https://doi.org/10.1063/5.0049591.
[66] I. Bhugun, J.M. Savéant, Derivatization of surfaces and self-inhibition in irreversible electrochemical reactions: cyclic voltammetry and preparative-scale electrolysis, J. Electroanal. Chem. 395 (1995) 127–131, https://doi.org/10.1016/0022-0728(95)04145-E.